J. Fluid Mech. (2000), *vol.* 425, *pp.* 235–258. Printed in the United Kingdom

Surfactant transport on mucus films

By R. V. CRASTER[1] AND O. K. MATAR[2]

[1]Department of Mathematics, Imperial College of Science, Technology and Medicine, London, SW7 2BZ, UK

[2]Department of Chemical Engineering and Chemical Technology, Imperial College of Science, Technology and Medicine, London, SW7 2BY, UK

(Received 21 December 1999 and in revised form 28 July 2000)

Motivated by the non-Newtonian properties of mucus and the bilayer nature of fluid lining in the pulmonary airways, we investigate surfactant transport on both single and bilayer fluid systems; the aim is twofold. First, we explore the influence of two principle rheological properties of mucus, yield stress and shear thinning, on the surfactant spreading behaviour. Secondly, in these airways, mucus, which has substantial non-Newtonian properties, overlies the periciliary liquid layer (PCL) which is primarily Newtonian, and we incorporate this bilayer structure into the analysis. This consists of the derivation of coupled spatio-temporal evolution equations describing the layer thicknesses and surfactant concentration. Subsequent analytical methods examine limiting cases where similarity variables can be usefully employed, and more generally numerical simulations are performed.

1. Introduction

Modelling the transport of surfactant within the lung under the action of Marangoni forces is a subject that has been extensively discussed in the literature, primarily by Grotberg and co-workers (Borgas & Grotberg 1988; Gaver & Grotberg 1990, 1992; Halpern & Grotberg 1992; Jensen & Grotberg 1992, 1993; Grotberg 1994; Grotberg, Halpern & Jensen 1995; Halpern, Jensen & Grotberg 1998) and Espinosa, Kamm and co-workers (Espinosa 1991; Espinosa *et al.* 1993; Espinosa & Kamm 1997, 1999). These studies are primarily motivated by the need to achieve a fundamental understanding of the spreading process in relation to surfactant replacement therapy (SRT) (Shapiro 1989). This is a method of treatment of respiratory distress syndrome (RDS) which occurs frequently in prematurely born infants with inadequate quantities of pulmonary surfactant (Robertson 1984) and proceeds via the external delivery of surfactant. The results of the existing theoretical models, which account for Marangoni stresses, surface diffusion, gravity, capillarity, solubility, intermolecular forces and the presence of an endogenous surfactant compare favourably with experimental observations for Newtonian fluids (Gaver & Grotberg 1992; Matar & Troian 1998; Bull *et al.* 1999; Dussaud, Matar & Troian 1999).

Nonetheless there do appear to be some aspects of this important problem that have remained hitherto unexplored. The effect of the rheological characteristics of the liquid film lining the inside of pulmonary airways on surfactant transport and a detailed incorporation of the bilayer nature of this lining constitute notable examples; our aim is to provide the relevant analysis.

The underlying motivation for this study is the observation that the liquid lung lining is not a single Newtonian fluid layer. First, the airway surface liquid is a

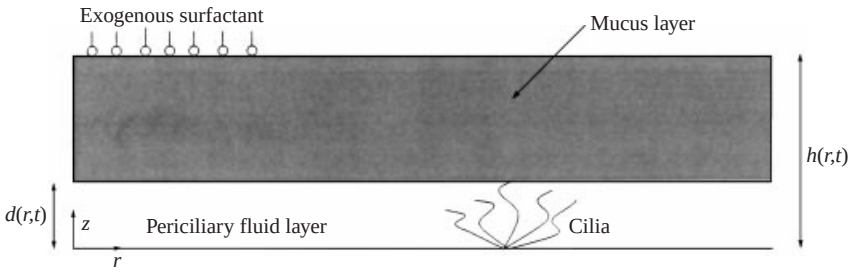

FIGURE 1. A sketch showing the geometry under consideration.

bilayer system, that is, the mucus layer overlies the periciliary liquid (PCL) layer. In the absence of reliable experimental work which could provide precise values for the thicknesses of the mucus and PCL layers, their relative thickness was estimated from data concerning the linings of bovine tracheal airways found in Widdicombe *et al.* (1997). This work states that 'The airways are lined with a film of fluid, which is 5–20 μm deep in healthy individuals', while the depth of the PCL does not exceed the length of the cilia, which is approximately equal to 6 μm. In the present study, we have taken the upper three-quarters of the height of the bilayer to consist of mucus; this 3 : 1 ratio is chosen to be illustrative rather than definitive. Some authors (Sleigh 1991) suggest that within the smaller airways, for which spreading by Marangoni forces is the dominant mode of surfactant transport, the proportion of mucus to PCL is actually much lower, and indeed the mucus layer could perhaps be even discontinuous. In the absence of conclusive experimental evidence from small human airways, we will use the tracheal values we estimate from Widdicombe *et al.* (1997) and simply note that future experiments may lead us, or others, to revisit this issue; it is important to also realise that some clinical conditions, such as cystic fibrosis, involve deep mucus layers for which this study will also be relevant. Furthermore, we will only examine spreading of surfactant on a continuous mucus layer.

The PCL consists of a watery less-viscous material occupied by the cilia, see figure 1; in normal lung function the cilia oscillate and their tips touch the base of the mucus layer propelling the overlying mucus, and any particles trapped within it, toward the trachea. The two layers appear to be strongly coupled with the mucus layer and PCL both flowing (Matsui *et al.* 1998). Thus the lower viscosity PCL can act as a lubricating layer and may affect conclusions based upon models which ignore it. Attention is focused on the potential influence of the two-layer system, wherein the material properties are markedly different, upon the results deduced for a single-layer system.

Secondly, despite the difficulties in collecting and analysing 'normal' mucus it is clear that mucus is a non-Newtonian fluid (Yeates 1991). Indeed many studies (Quraishi, Jones & Mason 1998 and references therein) suggest that nasal and lung mucus are markedly non-Newtonian with an appreciable elasticity (measured by the 'spinnability'), shear thinning, thixotropy, and a yield stress (Davis 1973; Basser, McMahon & Griffith 1989); the latter is required to carry the particulate debris which are to be removed from the lung. Moreover, different diseases and situations can cause wide variations in the measured material properties. The issues connected with non-Newtonian properties are not currently addressed by the mathematical models available, although there is mention in the literature of the importance of mucus rheology in neonatal respiratory distress syndrome (Rubin, Ramirez & King 1992). Although this study is primarily motivated by a need to accurately

model the spreading process in connection with SRT, interest also exists in bilayer thin films in industrial coating processes; often materials, such as paints, have an appreciable non-Newtonian behaviour (Barnes 1999). To ascertain the importance of non-Newtonian behaviour we utilize yield-stress, shear-thinning materials using as our rheological model the Herschel–Bulkley constitutive law (Herschel & Bulkley 1923). It is important to appreciate that mucus undoubtedly has viscoelastic behaviour, and that the surfactant itself may alter the material properties such as yield stress and viscoelastic parameters (Rubin *et al.* 1992), but we shall leave the yet further complicating aspects of those issues for future work.

The analysis in this paper relies upon utilizing the remarkably thin fluid layers that exist in the lung lining, which leads naturally to lubrication theory; the basic formulation for a bilayer film, relevant scaling, and thin-layer expansion are given in §§ 2, 3 and 4, respectively. A brief analytical study based upon similarity variables is presented in § 5 and we then collect together our numerical results in § 6. There we consider a single layer of yield-stress, shear-thinning material in § 6.1 with the equivalent bilayer system being considered in § 6.2. Finally, in § 7 we provide some concluding remarks.

2. Formulation

We now formulate the problem of a thin bilayer system of immiscible Herschel–Bulkley materials.

2.1. *The governing equations*

Two thin films of incompressible material lie on a flat horizontal plane (the cell surface). Exogenous surfactant is introduced at the free surface and the resultant flow is induced by surface tension gradients that arise due to the presence of gradients in surfactant concentration. This so-called Marangoni flow occurs in the direction of the uncontaminated mucus layer as shown in figure 1, which depicts the geometry of flow. For definiteness we shall initially assume axisymmetry, although the analysis is easily adapted to planar configurations; a unified notation will be adopted following non-dimensionalization. Fluid motion is described by the velocity field, $(u(r,z,t),0,w(r,z,t))$, in cylindrical polar co-ordinates with origin coincident with the centre of applied surfactant, as shown in figure 1, while pressure is denoted by $p(r,z,t)$; the mucus and PCL layers have density ρ and ρ_d, respectively. The total fluid height is $h(r,t)$ and the PCL layer has height $d(r,t)$; all material variables associated with the PCL have the distinguishing subscript d.

The equations for the film in the upper layer are given by conservation of momentum,

$$u_t + uu_r + wu_z = -\frac{1}{\rho}p_r + \frac{1}{\rho}\left[\tau_{rr,r} + \tau_{rz,z} + \frac{1}{r}(\tau_{rr} - \tau_{\theta\theta})\right], \tag{2.1}$$

$$w_t + uw_r + ww_z = -\frac{1}{\rho}p_z - g + \frac{1}{\rho}\left[\tau_{zr,r} + \tau_{zz,z} + \frac{\tau_{rz}}{r}\right], \tag{2.2}$$

and continuity,

$$\partial_r(u) + w_z = 0, \tag{2.3}$$

where τ_{ij} denotes the components of the deviatoric stress tensor and the subscripts (r,z,t) denote partial derivatives, except in the case of derivatives of the stress components, $\tau_{ij,j}$, where the last subscript refers to the derivative. For axisymmetric

geometry we use the notation $\partial_r(\ ) \equiv r^{-1}(r[\ ])_r$. For a visco-plastic fluid, these stresses are related to the strain rates through a constitutive model, which will be discussed shortly. The equations for the lower layer are identical, but with the addition of the d subscripts to distinguish different material parameters.

The concentration of surfactant, $\Gamma(r,t)$, satisfies a surface transport equation

$$\Gamma_t + \nabla_s \cdot (\boldsymbol{u}_s \Gamma) + (\nabla_s \cdot \boldsymbol{n})\Gamma(\boldsymbol{u} \cdot \boldsymbol{n}) = \mathscr{D}\nabla_s^2 \Gamma + J \tag{2.4}$$

on $z = h(r,t)$; a derivation and discussion of the physical meaning of the terms in this equation can be found in Stone (1990). Equation (2.4) contains gradient operators defined on the surface: the surface gradient operator, ∇_s, is $\nabla_s = [\boldsymbol{I} - \boldsymbol{n}\boldsymbol{n}] \cdot \nabla \equiv \boldsymbol{I}_s \cdot \nabla$ and $\boldsymbol{u}_s$ is the surface velocity: $\boldsymbol{u}_s = \boldsymbol{I}_s \cdot \boldsymbol{u}$. In addition, the term $\mathscr{D}$ is a measure of surface diffusion and J represents the flux of material to the interface – a term which is henceforth ignored.

In this paper it is assumed that the surfactant is insoluble in the mucus. Hence equation (2.4) is not coupled to a concentration advection–diffusion equation in the bulk. The governing equations are coupled to an equation of state which relates the surface tension to the surfactant concentration. These equations are solved subject to the following boundary conditions:

no-slip at the solid substrate,

$$u = 0 \quad \text{and} \quad w = 0 \quad \text{on } z = 0, \tag{2.5}$$

and at the mucus–air interface, $z = h(r,t)$,

$$h_t + u h_r = w. \tag{2.6}$$

The Boussinesq–Scriven description of a Newtonian interface (Edwards, Brenner & Wasan 1991) is adopted which introduces an extra stress tensor, $\boldsymbol{\tau}_s$,

$$\boldsymbol{n} \cdot \boldsymbol{\tau}_s = -\sigma(\nabla_s \cdot \boldsymbol{n})\boldsymbol{n} + \nabla_s \sigma, \tag{2.7}$$

into the free-surface boundary condition. In (2.7) the surface tension, σ, and the normal to the free surface, $\boldsymbol{n} = (-h_r, 0, 1)/\sqrt{h_r^2 + 1}$, naturally appear in the extra stress equation. Provided contributions due to the surface viscosities are neglected, the free-surface boundary condition, at $z = h(r,t)$, is expressed by

$$\boldsymbol{n} \cdot (\boldsymbol{\tau} - \boldsymbol{I}p) = \boldsymbol{n} \cdot \boldsymbol{\tau}_s. \tag{2.8}$$

At the mucus–PCL interface, $z = d(r,t)$, the velocities are continuous as is $\boldsymbol{n}\cdot(\boldsymbol{\tau} - p\boldsymbol{I})$; we additionally assume that there are no surfactants at $z = d(r,t)$ and hence no surface tension gradients or surface viscosities acting at this interface. Surface tension could be included into the interfacial boundary condition, but as the surfactant at the air–liquid interface is assumed insoluble there will be no gradients of surface tension at $z = d(r,t)$, and the curvature-dependent term will become a higher-order contribution after the later scalings are applied. We therefore choose to omit this from the analysis at the outset by assuming that there are no interfacial surface tension effects. Moreover we assume that the density of the lower layer is greater than that of the upper layer to prevent buoyancy-driven convection.

2.2. *Rheology*

As discussed earlier two important rheological properties of mucus are yield stress and shear thinning; undoubtedly also important are viscoelastic properties, but we concentrate upon modelling the former. Mucus is composed of a network of cross-linked mucins (Moriarty & Grotberg 1999; Wu & Carlson 1991) and this structure

Constants	Mucus values	Source
Viscosity†, λ (P)	10^{-2}–10^{2}	Silberberg (1983)
Yield stress, τ_p (dyn cm^{-2})	10^{3}	Silberberg (1983)
Layer thickness, $\mathscr{H}$ (cm)	10^{-4}	Widdicombe *et al.* (1997)
Length scale, $\mathscr{L}$ (cm)	10^{-2}	Jensen (1994)
Density, ρ (g cm^{-3})	1	$\sim$ Water
Spreading pressure, $\mathscr{S}$ (dyn cm^{-1})	10	Rubin *et al.* (1992)
Gravity, g (cm s^{-2})	981	
Surface diffusivity‡, $\mathscr{D}$ (cm^2 s^{-1})	10^{-6}–10^{-4}	Sakata & Berg (1969)
Power law exponent, n	0.3–0.5	Basser *et al.* (1989)

TABLE 1. Order-of-magnitude estimates for the physical constants associated with mucus where the data are taken, or estimated, from a variety of sources. † For viscosity, the lower value is that of water and the higher ranges of viscosity in part reflect those due to a variety of medical conditions and are additionally estimated from the results in Silberberg (1983); PCL is taken to have viscosity 10^{-2} P. ‡ The diffusivities take a range of values around 10^{-5} which is the typical value taken by Sakata & Berg (1969).

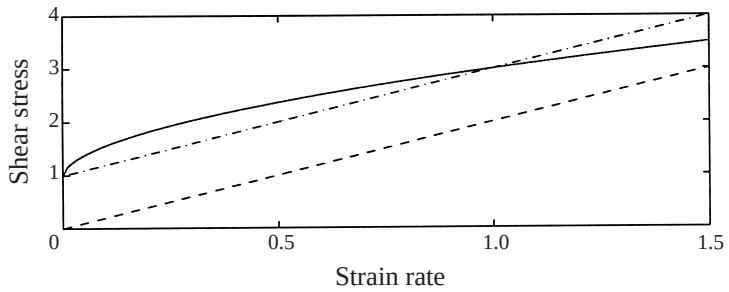

FIGURE 2. A sketch of the constitutive relations for the Bingham fluid (dot-dashed line), a Newtonian fluid (dashed line) and a Herschel–Bulkley material with $n < 1$ (solid line) for simple shear; the scales are arbitrary.

endows mucus with an inherent strength – hence the yield stress which can be substantial (see table 1). During flow this structure is progressively broken down leading to the nonlinear dependence of shear rate upon the the applied shear. A rheological model widely used in chemical engineering to capture this behaviour for yield stress materials, often leading to very accurate predictions, is the Herschel–Bulkley model (Herschel & Bulkley 1923; Sherwood & Durban 1998); some recent applications from geophysical flows with comparisons between experiment and theory are in Coussot (1994), Huang & Garcia (1998), and Balmforth *et al.* (2000). We adopt the Herschel–Bulkley model herein:

$$\tau_{ij} = \left(K\dot{\gamma}^{n-1} + \frac{\tau_p}{\dot{\gamma}} \right) \dot{\gamma}_{ij} \quad \text{for } \tau \geqslant \tau_p \qquad \text{and} \qquad \dot{\gamma}_{ij} = 0 \quad \text{for } \tau < \tau_p. \tag{2.9}$$

The second invariants of the deviatoric stress tensor, τ_{ij}, and the strain-rate tensor, $\dot{\gamma}_{ij}$, are defined as $\tau = \sqrt{\tau_{jk}\tau_{jk}/2}$ and $\dot{\gamma} = \sqrt{\dot{\gamma}_{jk}\dot{\gamma}_{jk}/2}$. The yield stress is τ_p, and K is the consistency; the model only allows flow to occur if the yield stress is exceeded. A sketch of the stress–strain-rate relations is shown in figure 2. There is a slightly simpler rheological model, the Bingham material, wherein once the yield stress is exceeded, then deviatoric stress is directly proportional to the shear rate; thus $n = 1$

and $K = \lambda = \rho\nu$, where λ is the plastic viscosity and ν is the kinematic viscosity. Hence, in this case, K is just conventional viscosity. In general, K provides a measure of resistance to shear. The parameter n characterizing the nonlinearity in the flow regime determines whether the fluid is shear thickening ($n > 1$) or shear thinning ($n < 1$), the latter being more relevant here (Basser *et al.* 1989).

3. Non-dimensionalization

The above equations are rendered dimensionless as follows. A characteristic thickness of the fluid layer, $\mathscr{H}$, is taken as the dimension of z, and $\mathscr{L}$ denotes a characteristic horizontal length scale. We measure the speed u by $\mathscr{V}$, and w by $\mathscr{H}\mathscr{V}/\mathscr{L}$, and time by $\mathscr{L}/\mathscr{V}$ so that,

$$r = \mathscr{L}\tilde{r}, \quad z = \mathscr{H}\tilde{z}, \quad u = \mathscr{V}\tilde{u}, \quad w = (\mathscr{V}\mathscr{H}/\mathscr{L})\tilde{w}, \quad t = (\mathscr{L}/\mathscr{V})\tilde{t} \quad \text{and} \quad h = \mathscr{H}\tilde{h}, \tag{3.1}$$

in which the tilde denotes dimensionless quantities. To non-dimensionalize the boundary conditions and equations involving the surfactant and surface tension we introduce

$$\sigma = \sigma_m + \mathscr{S}\tilde{\sigma}, \qquad \Gamma = \Gamma_m\tilde{\Gamma}. \tag{3.2}$$

The terms Γ_m and σ_m represent the saturation values of surfactant and surface tension; $\mathscr{S} = \sigma_0 - \sigma_m$ corresponds to the spreading pressure wherein σ_0 is the surface tension of a perfectly clean, surfactant-free interface.

For pressure we introduce $p = \mathscr{S}\tilde{p}/\mathscr{H}$, and, provided we use the Herschel–Bulkley model, then for general n we define

$$\lambda = \frac{K\mathscr{V}^{n-1}}{\mathscr{H}^{n-1}}. \tag{3.3}$$

We then select the characteristic velocity scale as

$$\mathscr{V} = \frac{\mathscr{S}\mathscr{H}}{\lambda\mathscr{L}}, \tag{3.4}$$

which expresses a balance between Marangoni stresses and viscous retardation. The strain rates and stresses scale as

$$\tau_{ij} = \frac{\lambda\mathscr{V}}{\mathscr{H}}\tilde{\tau}_{ij}, \qquad \dot{\gamma}_{ij} = \frac{\mathscr{V}}{\mathscr{H}}\tilde{\dot{\gamma}}_{ij}, \tag{3.5}$$

and are given in detail in equations (3.12) and (3.13).

On substituting the non-dimensional variables into the governing equations, and discarding the tilde, we arrive at the standard lubrication equations in the upper layer:

$$Re\,(u_t + uu_r + wu_z) = -p_r + \epsilon\tau_{rr,r} + \tau_{rz,z} + \epsilon\frac{1}{r}(\tau_{rr} - \tau_{\theta\theta}), \tag{3.6}$$

$$\epsilon^2 Re\,(w_t + uw_r + ww_z) = -p_z - \mathscr{G} + \epsilon^2\tau_{zr,r} + \epsilon\tau_{zz,z} + \epsilon^2\frac{\tau_{rz}}{r}, \tag{3.7}$$

$$\partial_r(u) + w_z = 0. \tag{3.8}$$

In the above equations, a number of non-dimensional parameters appear. These are $\epsilon = \mathscr{H}/\mathscr{L}$, the aspect ratio of the fluid layer, the Reynolds number, Re, and the Bond number, $\mathscr{G}$, which measures the relative importance of gravity versus surface tension

Non-dimensional parameter:	ϵ	Re	B	$\mathscr{G}$	Pe
Representation	$\mathscr{H}/\mathscr{L}$	$\rho\mathscr{H}\mathscr{V}^2/\mathscr{S}$	$\tau_p\mathscr{L}/\mathscr{S}$	$\rho g\mathscr{H}^2/\mathscr{S}$	$\mathscr{L}\mathscr{V}/\mathscr{D}$
Typical value	10^{-2}	10^{-7}–10	1	10^{-6}	1–10^5

TABLE 2. Typical values of non-dimensional numbers, given the physical constants in table 1.

gradients. These parameters are defined by

$$Re \equiv \frac{\rho\mathscr{H}\mathscr{V}^2}{\mathscr{S}}, \quad \text{and} \quad \mathscr{G} \equiv \frac{\rho g\mathscr{H}^2}{\mathscr{S}}, \tag{3.9}$$

and typical values are in table 2.

For a bilayer system we have another fluid in $0 < z < d$ where, as before, the subscript d on all material constants will denote those associated with the PCL layer:

$$\frac{\rho_d}{\rho} Re\,(u_t + uu_r + wu_z) = -p_r + \frac{\lambda_d}{\lambda}\left[\epsilon\tau_{rr,r} + \tau_{rz,z} + \epsilon\frac{1}{r}(\tau_{rr} - \tau_{\theta\theta})\right], \tag{3.10}$$

$$\epsilon^2\frac{\rho_d}{\rho} Re\,(w_t + uw_r + ww_z) = -p_z - \frac{\rho_d}{\rho}\mathscr{G} + \frac{\lambda_d}{\lambda}\left[\epsilon^2\tau_{zr,r} + \epsilon\tau_{zz,z} + \epsilon^2\frac{\tau_{rz}}{r}\right], \tag{3.11}$$

together with continuity as in (3.8).

In table 2 we summarize the main non-dimensional parameters of the problem together with order-of-magnitude estimates (based on the physical constants listed in table 1).

With the exception of the scaling adopted in (3.3), the development thus far parallels that of the Newtonian case with the stress–strain-rate constitutive relation as yet undetermined. We introduce the units $\mathscr{V}/\mathscr{H}$ for the strain rates so that the non-dimensional constitutive relations become

$$\dot{\gamma}_{ij} = \begin{pmatrix} 2\epsilon u_r & 0 & u_z + \epsilon^2 w_r \\ 0 & 2\epsilon u/r & 0 \\ u_z + \epsilon^2 w_r & 0 & 2\epsilon w_z \end{pmatrix}. \tag{3.12}$$

Using (3.12) and the dimension $\lambda\mathscr{V}/\mathscr{H}$ for τ_{ij}, we construct the dimensionless stress components through

$$\tau_{ij} = \left[\dot{\gamma}^{n-1} + \frac{B}{\dot{\gamma}}\right]\dot{\gamma}_{ij}, \tag{3.13}$$

in $d < z < h$, and if we so desired with n_d and B_d replacing their sister variables in $0 < z < d$. The relation (3.13) is valid provided $\tau > B$ ($\tau > B_d$), where a non-dimensional group parameterizing the characteristic yield stress, τ_p, emerges:

$$B = \frac{\tau_p\mathscr{H}}{\lambda\mathscr{V}} \equiv \frac{\tau_p\mathscr{L}}{\mathscr{S}}. \tag{3.14}$$

Otherwise, if $\tau < B$ the constitutive law suggests that $\dot{\gamma}_{ij} = 0$. We sometimes refer to B as the Bingham number, in analogy with the situation when $n = 1$. We shall not consider the PCL as having a yield stress; we shall neither define nor use a Bingham number in that layer.

The surface boundary conditions are

$$\left.\begin{aligned} h_t + uh_r &= w \\ \tau_{rz} + ph_r &= \epsilon h_r \tau_{rr} + \sigma_r \\ p &= \epsilon(\tau_{zz} - \epsilon h_r \tau_{rz}) \end{aligned}\right\} \quad \text{on } z = h(r,t). \tag{3.15}$$

In addition, the surfactant transport equation becomes

$$\Gamma_t + \partial_r(u_s \Gamma) = \frac{1}{Pe}\partial_r(\Gamma_r) + O(\epsilon) \tag{3.16}$$

with the surface Péclet number defined as $Pe = \mathscr{L}\mathscr{V}/\mathscr{D}$. Here u_s now denotes the radial component of the surface velocity. At the mucus–PCL interface, located at $z = d(r,t)$, the velocity is continuous and $d_t + ud_r = w$. The stress relations $\tau_{rz} + pd_r - \epsilon d_r \tau_{rr}$, $p - \epsilon(\tau_{zz} + \epsilon d_r \tau_{rz})$ are also continuous. The boundary conditions on $z = 0$ remain as $u = 0$ and $w = 0$.

4. The thin-layer equations

In this section, evolution equations for h, d and Γ are derived in the lubrication approximation within which only leading-order terms in ϵ are retained. In the governing momentum equations the curvature terms do not occur at this order, hence from hereon a notation which unifies axisymmetric, (r,z), and plane Cartesian, (x,z), geometries is adopted by defining a new variable η as

$$\eta = \begin{cases} x & \text{strip} \\ r & \text{drop} \end{cases}, \quad \partial_\eta[\,] = \begin{cases} \partial_x[\,] & \text{strip} \\ (1/r)\partial_r[r] & \text{drop} \end{cases}, \quad (\,)_\eta = \begin{cases} (\,)_x & \text{strip} \\ (\,)_r & \text{drop} \end{cases}. \tag{4.1}$$

Then

$$p_z = -\mathscr{G}, \qquad -p_\eta + \tau_{\eta z,z} = 0 \quad \text{in } d < z < h, \tag{4.2}$$

and

$$p_z = -\frac{\rho_d}{\rho}\mathscr{G}, \qquad -p_\eta + \frac{1}{\mu}\tau_{\eta z,z} = 0 \quad \text{in } 0 < z < d, \tag{4.3}$$

where $\mu = \lambda/\lambda_d$, and with boundary conditions on $z = h(\eta,t)$ that

$$h_t + uh_\eta = w, \quad \tau_{\eta z} = \sigma_\eta, \quad p = 0 + O(\epsilon^2), \tag{4.4}$$

wherein capillary effects have been neglected since they arise at $O(\epsilon^2)$ (Jensen & Grotberg 1993). In addition the surface transport equation

$$\Gamma_t + \partial_\eta(u_s \Gamma) = \frac{1}{Pe}\partial_\eta(\Gamma_\eta) \tag{4.5}$$

on $z = h(\eta,t)$ is required together with an equation of state relating the surfactant concentration to the surface tension. Note that even though $Pe \leqslant O(10^5)$ (as shown in table 2, that is, $1/Pe$ can be of order ϵ) we nevertheless retain surface diffusion effects in equation (4.5). We justify this by arguing that the parameter multiplies higher-derivative terms, giving the equations a singular perturbation; their omission leads to the non-smooth shock-like similarity solutions of § 5. These effects also provide an additional driving mechanism for spreading, endowing (4.5) with a parabolic character and giving rise to smooth solutions.

For an equation of state we choose to adopt the relation

$$\sigma(\Gamma) = (\beta+1)[1+\theta(\beta)\Gamma]^{-3} - \beta; \qquad \theta(\beta) = [(\beta+1)/\beta]^{1/3} - 1, \quad \beta = \sigma_m/S, \tag{4.6}$$

introduced by Sheludko (1967) and extensively used by Grotberg and co-workers; other equations of state based upon Langmuir or Frumkin isotherms could also be considered (Edwards *et al.* 1991). For $\beta \geqslant 5$ the equation of state yields solutions quantitatively little different from a linearized relationship. Since our subsequent numerical simulations are an investigation of rheological effects we shall in those sections take β to be large.

At the mucus–PCL interface $z = d(\eta, t)$ the velocity and pressure are continuous and

$$d_t + ud_\eta = w, \quad \mu\tau^+_{\eta z} = \tau^-_{\eta z}, \quad u^+ = u^- \qquad \text{on } z = d, \tag{4.7}$$

where the superscripts + and − denote the limiting values as we approach the interface from above and below respectively and the boundary conditions on $z = 0$ are simply that $u = 0$ and $w = 0$.

Inspection of the typical values listed in table 2 reveals that for the extremely thin layers in the current application $\mathscr{G} \ll 1$, indicating that gravity plays little role and is therefore neglected henceforth. Solution of (4.2) and (4.3) yields $p = 0$ and $\tau_{\eta z} = \sigma_\eta$ for $d < z < h$ and $\tau_{\eta z} = \mu\sigma_\eta$ for $0 < z < d$. Except for the viscosity (consistency) changes, these are independent of the constitutive relation which only comes into play when the stress is related to the strain rate whereupon it becomes evident that

$$u(\eta, z, t) = \begin{cases} [\sigma_\eta - B]_+^{1/n}(z-d) + (\mu\sigma_\eta)^{1/n_d} d & \text{in } d < z < h \\ (\mu\sigma_\eta)^{1/n_d} z & \text{in } 0 < z < d. \end{cases} \tag{4.8}$$

The function $[\sigma_\eta - B]_+$ is $\sigma_\eta - B$ for $\sigma_\eta > B$ and is zero otherwise. We now define the volume fluxes in the layer as

$$\mathscr{U}(\eta, t) = \int_0^h u(\eta, z, t)\,\mathrm{d}z \quad \text{and} \quad \mathscr{U}_d(\eta, t) = \int_0^d u(\eta, z, t)\,\mathrm{d}z \tag{4.9}$$

and hence from (4.8) that

$$\mathscr{U}(\eta, t) = [\sigma_\eta - B]_+^{1/n}\left[\tfrac{1}{2}(h^2 - d^2) - d(h-d)\right] + (\mu\sigma_\eta)^{1/n_d} d(h - d/2) \tag{4.10}$$

and

$$\mathscr{U}_d(\eta, t) = \frac{(\mu\sigma_\eta)^{1/n_d}}{2} d^2. \tag{4.11}$$

Utilizing the equation of continuity, the evolution equations for the heights of the layers are

$$h_t + \partial_\eta \mathscr{U}(\eta, t) = 0, \qquad d_t + \partial_\eta \mathscr{U}_d(\eta, t) = 0, \tag{4.12}$$

with the surfactant evolving according to

$$\Gamma_t + \partial_\eta[\Gamma([\sigma_\eta - B]_+^{1/n}(h-d) + (\mu\sigma_\eta)^{1/n_d} d)] = \frac{1}{Pe}\partial_\eta \Gamma_\eta. \tag{4.13}$$

Equations (4.12) and (4.13) govern the spatio-temporal evolution of $h(\eta, t)$, $d(\eta, t)$ and $\Gamma(\eta, t)$. These coupled evolution equations are now explored both analytically and numerically. In the absence of yield stress and if, furthermore, both layers have identical shear-thinning properties, that is $n = n_d$, then equations (4.12) can be combined to give

$$[h + (\mu^{1/n} - 1)d]_t + \tfrac{1}{2}\partial_\eta(\sigma_\eta^{1/n}[h + (\mu^{1/n} - 1)d]^2) = 0. \tag{4.14}$$

and equation (4.13) also contains the combination $h + (\mu^{1/n} - 1)d$.

5. Similarity solutions

In this section we shall derive similarity solutions of the first kind to describe the spreading process on bilayer systems. These solutions approximate the flow over large regions of the spatial domain and provide useful limiting relations for comparison with the numerical solutions discussed in § 6.

5.1. *Negligible yield stress* ($B = 0$)

It is evident that as $Pe \to \infty$ the evolution equations describing the dynamics of a single Newtonian or power-law fluid layer can admit similarity solutions (Jensen & Grotberg 1992; Jensen 1994). Similarity solutions also exist for bilayer (or multilayer) systems in the absence of yield stresses in which the nonlinearity associated with the shear-thinning rheology is identical in each layer, that is $n = n_d$; each layer only differs in its viscosity (consistency). The analysis required is ultimately similar to that of Jensen & Grotberg (1992), Jensen (1994); however we persist in briefly describing these solutions here, in part because the effect of shear thinning is to alter the characteristic scalings often quoted and used in surfactant spreading analyses, and in part because we shall compare these bilayer similarity solutions with the later numerical results.

In order to extract similarity solutions we linearize the equation of state (4.6) so that $\sigma_\eta \equiv -\Gamma_\eta$; then for a power-law fluid we use the similarity variable $\xi = \eta/[\xi_s t^a]$. The parameter ξ_s simply rescales the solutions so that the surfactant front is at $\xi = 1$; ξ_s is explicitly defined in equation (5.11). The variables are defined as $h(\eta, t) = H(\xi)$, $d(\eta, t) = D(\xi)$, and $\Gamma(\eta, t) = \xi_s^{1+n} G(\xi)/t^b$. Furthermore, it is convenient to define $J(\xi) = H(\xi) + (\mu^{1/n} - 1)D(\xi)$. Then with a total mass of surfactant Qt^α (the parameter α allows for an increasing amount of surfactant to be introduced) the powers a and b emerge (Jensen 1994) as

$$a = \frac{\alpha + n}{3 + n} \qquad \left(\text{or} \quad a = \frac{\alpha + n}{2 + n}\right), \tag{5.1}$$

$$b = \frac{(2 - \alpha)n - \alpha}{3 + n} \qquad \left(\text{or} \quad b = \frac{(1 - \alpha)n - \alpha}{2 + n}\right). \tag{5.2}$$

These results are for a spreading drop (or a strip). It is worthy of mention that a boundedness constraint on Γ imposes the restriction $b \geqslant 0$ from which the following constraint is imposed on α: $\alpha \leqslant 2n/(1+n)$ (or $\alpha \leqslant n/(1+n)$ in rectilinear coordinates). The limit $n = 0$ is analogous to a yield-stress-dominated layer; here the scalings are $a = \alpha/3, b = -\alpha/3$ and for a fixed initial mass of surfactant these are zero and the spreading process stops. For brevity hereon we just consider the spreading rate of a fixed mass of surfactant $\alpha = 0$, then shear thinning has $n < 1$. From values estimated from Basser *et al.* (1989) for their mucus analogue material a value of $n = 1/2$ for the flow index appears reasonable; then, for that value, $t^{1/7}$ is the spreading rate rather than the conventional Newtonian value $t^{1/4}$; in general shear thinning markedly slows the distribution of surfactant.

The bilayer equations rescale using the similarity transformation to

$$a(\xi^2 G)_\xi - [\xi G J(-G_\xi)^{1/n}]_\xi = 0, \quad (\text{or} \quad a(\xi G)_\xi - [G J(-G_\xi)^{1/n}]_\xi = 0), \tag{5.3}$$

$$a\xi J_\xi - \tfrac{1}{2}\partial_\xi [J^2(-G_\xi)^{1/n}] = 0, \quad a\xi D_\xi - \tfrac{1}{2}\mu^{1/n}\partial_\xi [D^2(-G_\xi)^{1/n}] = 0, \tag{5.4}$$

with the notation for ∂_ξ and $(\,)_\xi$ following from (4.1). The first equation integrates to

give

$$G_\xi = -\left(\frac{a\xi}{J}\right)^n \Theta(1-\xi), \tag{5.5}$$

where $\Theta(1-\xi)$ is the Heaviside function defined to be zero for $\xi > 1$ and one otherwise. With the boundary conditions on $\xi > 1$ that $H = 1$, $G = 0$ and $D = d_0$ (< 1) then the solutions for $\xi < 1$ are that

$$G(\xi) = -\left(\frac{a}{2J_-}\right)^n \frac{(\xi^{1-n}-1)}{(1-n)} \qquad \left(\text{or} \quad G(\xi) = -\left(\frac{a}{2J_-}\right)^n (\xi - 1)\right), \tag{5.6}$$

for $\xi < 1$ in which the parameter $J_- = [1 + (\mu^{1/n} - 1)d_0]$ and

$$J(\xi) = 2J_-\xi^2 \qquad (\text{or} \quad J(\xi) = 2J_-\xi), \tag{5.7}$$

and

$$D(\xi) = \frac{2J_-}{\mu^{1/n}}\left(1 - \left(1 - \frac{\mu^{1/n}d_0}{J_-}\right)^{1/2}\right), \tag{5.8}$$

that is, $D(\xi)$ is simply a constant, or

$$D(\xi) = \frac{2J_-}{\mu^{1/n}}\xi^2 \qquad \left(\text{or} \quad \frac{2J_-}{\mu^{1/n}}\xi\right). \tag{5.9}$$

This latter solution is inconsistent with the jump conditions at the shock, unless the mucus is completely absent and $d_0 = 1$, but it does play a role in some of the later solutions. It additionally implies that for some value of ξ bounded below by

$$\xi^2 = \frac{1}{2}\left(1 - \left(1 - \frac{2\mu^{1/n}d_0}{J_-}\right)^{1/2}\right) \tag{5.10}$$

and above by one then, for the strip solution, for instance, the constant solution will revert to (5.9). The height field follows from $J(\xi)$ and the scaling variable ξ_s is

$$\xi_s = \left[\frac{2Q(3-n)}{(a/2J_-)^n}\right]^{1/(3+n)} \qquad \left(\text{or} \quad \xi_s = \left[\frac{2Q}{(a/2J_-)^n}\right]^{1/(2+n)}\right), \tag{5.11}$$

which requires the initial mass of surfactant to be conserved, with the choice of initial condition chosen in the numerical work (§ 6)

$$Q = 1/2 \quad \left(\text{or} \quad Q = \sqrt{\pi}/2\right).$$

5.2. *Large yield stress* ($B \gg 1$)

Once again we concentrate upon the analysis for a finite mass of deposited surfactant, but now in the mucus layer we consider $B \gg 1$ (or equivalently $n \ll 1$). The similarity equations now become

$$a\xi D_\xi - \frac{\mu^{1/n_d}}{2}\partial_\xi[(-G_\xi)^{1/n_d}D^2] = 0, \tag{5.12}$$

$$a(\xi^2 G)_\xi - \mu^{1/n_d}[\xi G\, D(-G_\xi)^{1/n_d}]_\xi = 0 \quad (\text{or} \quad a(\xi G)_\xi - \mu^{1/n_d}[G\, D(-G_\xi)^{1/n_d}]_\xi = 0), \tag{5.13}$$

$$a\xi H_\xi - \mu^{1/n_d}\partial_\xi\left[(-G_\xi)^{1/n_d}D\left(H - \frac{D}{2}\right)\right] = 0. \tag{5.14}$$

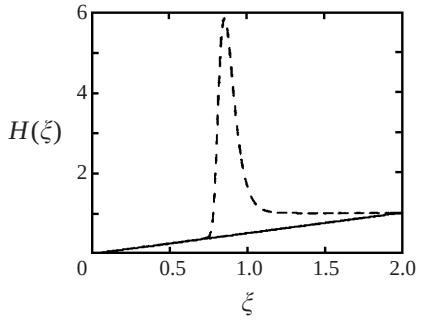

FIGURE 3. The height profile, shown as a dashed line, for a yield-stress-dominated layer versus the similarity variable; the solid line shows $2\xi d_0$. The parameter values are $\mu = 1$, $n_d = 1$ and $\varepsilon = 0.1$.

Notably, the height variable, $H(\xi)$, does not appear in the PCL height and surfactant evolution equations, (5.12) and (5.13). These remain coupled and can be solved independently with their solutions driving the height evolution equation (5.14).

Equation (5.13) can be integrated directly yielding (5.5) for G_ξ, but with J replaced by $\mu^{1/n_d} D(\xi)$. The natural way of dealing with the height evolution equation, (5.14), which is driven by functions that suddenly change character when $\xi < 1$, is via generalized functions. Substitution of a trial solution of the form $D(\xi) = d_0\,[f_1(\xi)\Theta(1-\xi) + [1 - \Theta(1-\xi)]]$ along with (5.5) into (5.12) yields $f_1(\xi) = 2\xi^2$ (or $f_1(\xi) = 2\xi$ for the strip case) as we naturally expect (Jensen & Grotberg 1992), so that we may express the solution generally as

$$D(\xi) = d_0[2\xi^{m+1}\Theta(1-\xi) + [1 - \Theta(1-\xi)]], \tag{5.15}$$

wherein m is a geometric parameter such that $m = 0$ for rectilinear geometry and $m = 1$ for the axisymmetric case. Substitution of $H(\xi) = f_2(\xi)\Theta(1-\xi) + (1 - f_3(\xi))$, along with the solutions for D and G_ξ into (5.14) yields

$$H(\xi) = 2d_0\xi^{m+1}\Theta(1-\xi) + \frac{(1-d_0)}{m+1}\delta(1-\xi) + [1 - \Theta(1-\xi)], \tag{5.16}$$

in which $\delta(1-\xi)$ is the Dirac delta function. Initially this infinite jump at the shock position appears disturbing; however it is in agreement with the integration of the governing equation across the jump at $\xi = 1$. Thus both $D(\xi)$ and $G(\xi)$ follow the usual Newtonian results suitably rescaled, whereas (5.16) predicts the development of a sharp peak in the height profile at the surfactant leading edge in this particular limit, $B \gg 1$. That is, in this limit, for $\xi < 1$ the mucus layer apparently disappears and becomes concentrated at the point $\xi = 1$ before adjusting to $H = 1$ for $\xi > 1$.

In reality, however, the presence of surface diffusion partially smooths these sharp cut-offs and to investigate the solution in the neighbourhood of $\xi = 1$ we regularize the Θ and δ terms by redefining $\Theta(1-\xi)$ as

$$\Theta(1-\xi) \sim \frac{1}{2}\left(\tanh\left[\frac{1-\xi}{\varepsilon}\right] + 1\right) \tag{5.17}$$

for some $\varepsilon \ll 1$ where ε is the regularization parameter. The δ-function is defined from the derivative of $\Theta(1-\xi)$. Integrating the equation (5.17) numerically backwards from large ξ where $H = 1$ leads to height profiles such as that shown in figure 3; the large peak at $\xi = 1$ (which can be made arbitrarily large by reducing ε) emerges due to the $\Theta(\xi - 1)$ and $\delta(1-\xi)$ terms as predicted by (5.16). These predictions are also

confirmed by numerical simulations of the full governing evolution equations; these are discussed in § 6.

5.3. *Physical balances*

An alternative analysis based upon dimensional scalings involves balancing the driving forces against those restraining motion. The latter are shear stresses integrated over the basal region beneath the induced flow

$$F_B \sim \lambda R^2 \dot{\gamma}^n \qquad (\text{or} \quad F_B \sim \lambda \mathscr{L} \dot{\gamma}^n), \tag{5.18}$$

where we use the length scales R and $\mathscr{L}$ to distinguish between the axisymmetric and strip geometries respectively, and the strain rates are

$$\dot{\gamma} \sim R/T\mathscr{H} \qquad (\text{or} \quad \dot{\gamma} \sim \mathscr{L}/T\mathscr{H}). \tag{5.19}$$

The driving forces are the surface tension gradients integrated over the area occupied by surfactant

$$F_D \sim \Gamma R \qquad (\text{or} \quad F_D \sim \Gamma). \tag{5.20}$$

There is also the mass constraint that

$$QT^{\alpha} \sim \Gamma R^2 \qquad (\text{or} \quad QT^{\alpha} \sim \Gamma \mathscr{L}). \tag{5.21}$$

Balancing the forces subject to that constraint recovers the basic scalings in equations (5.1), (5.2). It is evident from balancing forces that a bilayer system will not alter these basic scalings, unless the nonlinearity of the restraining forces differs in each layer.

6. Numerical results

The coupled evolution equations (4.12) and (4.13) are now solved numerically using an adaptive grid scheme; the scheme is specifically designed to solve nonlinear parabolic equations, and is described in some detail by Blom & Zegeling (1994). It has been successfully utilized in other situations involving rapidly changing solutions, and highly nonlinear governing equations, for instance in tracking splitting pulses in chemical autocatalysis (Doelman, Kaper & Zegeling 1997) and related instability problems (Balmforth, Craster & Malham 1999). Thus we have confidence in its ability to deal with the current numerical difficulties, including the shock-like structure. The only minor change is that we choose to adapt the grid ignoring the surfactant concentration, and adapt it using only the total and PCL height profiles; this ensures that we concentrate most points at the most severe changes in the spatial gradients, particularly in the neighbourhood of the shock-like structure at the surfactant leading edge. As a further consistency check upon the accuracy of the numerical simulations we also performed comparative evaluations using a finite-element collocation scheme (Keast & Muir 1991) and related numerical schemes using finite differences (Matar & Troian 1999*a*, *b*); the results were virtually indistinguishable in each case although the finite-element calculations required double the number of grid points than the adaptive scheme to obtain the same relative accuracy. Typically we employed two thousand grid points on a computational domain of length ten.

One convenient approach (Jensen & Grotberg 1992; Matar & Troian 1999*a*) is to move the numerical scheme to a frame of reference where one utilizes the similarity variable. We do not adopt this line of attack here as the yield stress, and differing power-law exponents in the PCL and mucus layers, break this self-similar scaling, and in some cases the solutions become stationary. We do, however, compare our

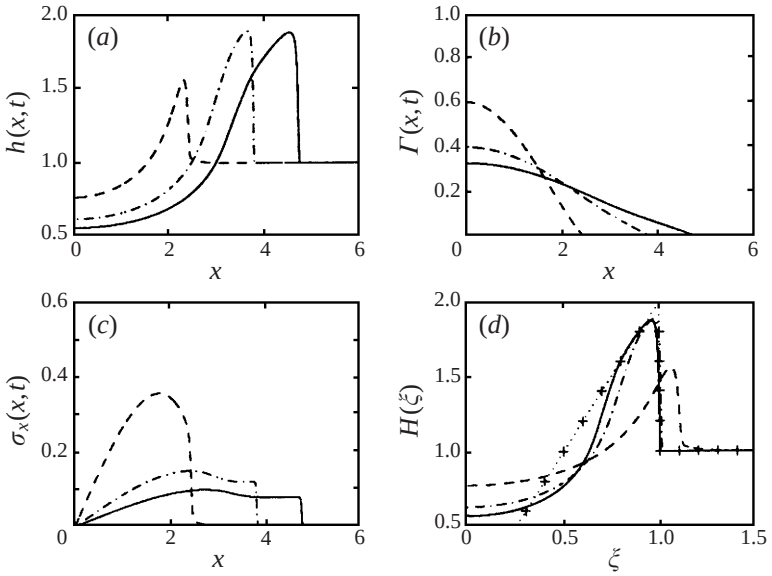

FIGURE 4. The Newtonian case: simulation for a strip with $Pe = 1000, \beta = 1000, n = 1, B = 0$. The solution is shown at times $t = 1$ (dashed), $t = 5$ (dot-dash) and $t = 10$ (solid line). (*a*), (*b*) and (*c*) The evolution of the height of the mucus layer, surfactant concentration and surface tension gradient respectively with time. (*d*) The height versus the Newtonian similarity coordinate, and the similarity solution is shown as $\cdots + \cdots$.

numerical solutions with the predictions of the similarity solutions derived analytically in § 5.

Spreading is forced by the initial conditions which in the computations we take to be

$$\Gamma(\eta, 0) = \exp(-\eta^2), \quad h(\eta, 0) = 1, \quad d(\eta, 0) = d_0, \tag{6.1}$$

where d_0 is a constant height with $0 < d_0 < 1$. Initial conditions which are similar in form to (6.1) have previously been used to provide a smooth approximation to the concentration of surfactant within a monolayer (Jensen & Grotberg 1992). We also specify that the first spatial derivatives of Γ, h and d all vanish at the origin. At a point η_∞ that is effectively at infinity (most figures have the rightmost η-axis value as 6; however the numerical grid extends out, at least, to $\eta = 10$) $\Gamma_\eta(\eta_\infty, t) = 0$ and the heights remain at their undisturbed initial values. We also fix the Péclet number to be $Pe = 1000$. This choice of Pe is in line with the scalings deduced earlier and corresponds to a primarily Marangoni-driven spreading process with corrections due to surface diffusion. Larger values of Pe lead to rapidly varying spatial gradients which are potentially more difficult to resolve accurately, while lower values are not entirely representative of typical spreading conditions; the rapid changes in the height profile at the surfactant front are reduced slightly as the Péclet number decreases. Computations are performed for times up to $t = 40$–100. These values are chosen to be long enough to enable comparisons with the self-similar solutions.

6.1. *Single layer*

We now systematically explore the various rheological cases within the single-layer context. As a preliminary step, however, we also provide results of numerical simulations for the Newtonian case ($B = 0$ and $n = 1$), shown in figure 4, for comparative

purposes. Particularly prominent in figure 4 is the shock feature at the surfactant leading edge. Although lubrication theory may be violated within this narrow region, with neglected terms providing first-order contributions, the model still provides an accurate representation of the majority of the flow.

The dimensionless times, 1, 5 and 10, at which we display the results in figure 4 show the evolution of the solution towards that given by the similarity analysis. We use the same choices of times in most subsequent figures; at a dimensionless time of 10 the solutions have evolved sufficiently that they are no longer dependent upon the initial condition, and, where they exist, similarity solutions are then approached. Those figures including a longer time, are those for which this convergence took noticeably longer. A comprehensive analysis of the Newtonian results have been presented by Jensen & Grotberg (1992); further discussion of these results is omitted from the present work.

6.1.1. *Effect of B* ($n = 1$)

We fix the power-law parameter, n, such that $n = 1$ and vary B, thus exploring yield stress. Typical results for this scenario with $B = 0.2$ are shown in figure 5; for other values of B one ultimately obtains solutions which follow a qualitatively similar physical evolution.

The effect of a yield stress is to restrain motion such that if at the free surface $\sigma_\eta(\eta, t) < B$, then there is no flow at that value of η. Following the thin-layer theory above, $u(\eta, z, t) = [\sigma_\eta - B]_+^{1/n} z$, thus those specific η where $\sigma_\eta = B$ separate regions of flow from those which are static; incidentally this is completely different from the situation that arises in gravity current flows of yield-stress materials such as muds or lavas (Liu & Mei 1989; Balmforth & Craster 1999; Balmforth *et al.* 1999) where a weakly yielded plug region rides atop flowing material. In the present situation there are unyielded regions and atop these regions the surfactant moves along the surface purely by diffusion; thus a strong yield stress effectively restricts surfactant from moving outside these regions. In particular, the initial surfactant profile must have gradients sharp enough to initiate flow for anything other than pure diffusion to take place. It is notable that the yielding behaviour is not dependent upon the surface tension itself, but the crucial quantity is the surface tension gradient. Also, the surface diffusion together with advection acts to decrease the surface tension gradient and hence the height profiles eventually become 'frozen' in place. Inspection of the numerical solution for the film height and the position of the front (the location of the surfactant leading edge), shown in figures 5(*a*) and 5(*d*), respectively, reveals that both the evolution of the film thickness and the spreading rate gradually stop; the height profiles remain fixed at the position shown for $t = 10$. The surfactant, on the other hand, is initially swept along by the flow, but ultimately moves by diffusion. More revealing is the surface tension gradient shown in figure 5(*c*): at $t = 10$ the majority of the material is still yielding, but only imperceptibly and the surface velocity, shown in figure 5(*e*), is negligible. Figure 5(*d*) shows the front position, that is the point at which the height adjusts to undisturbed conditions at the surfactant leading edge, and simply illustrates that the usual Newtonian similarity scaling of $t^{1/3}$ for the strip case is initially followed by these flows, but is ultimately not adhered to, and eventually flow ceases.

One initially odd feature of figure 5(*a*) is the sharp peak in the height profile near the origin, which might lead one to assume that the boundary condition $h_\eta(\eta, 0)$ has been violated. In fact, however, the condition is maintained very close to the origin and this feature emerges as the surface tension gradient is locally zero there; thus the

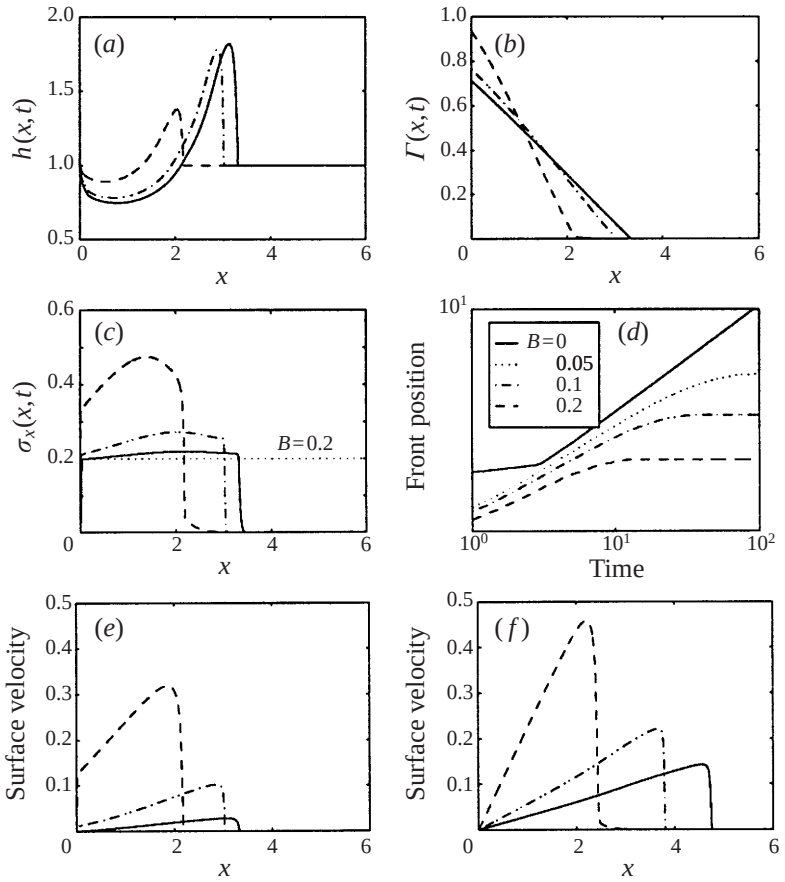

FIGURE 5. The yield stress case: simulation for a strip with $Pe = 1000, \beta = 1000, n = 1, B = 0.2$. The solution is shown at times $t = 1$ (dashed), $t = 5$ (dot-dash) and $t = 10$ (solid line). (*a*), (*b*) and (*c*) The evolution of the height of the mucus layer, surfactant concentration and surface tension gradient respectively with time. (*d*) The front position versus time for several values of B. (*e*) The surface velocity for the Bingham simulation, and for comparative purposes the Newtonian velocity is shown in (*f*).

yield stress only allows surfactant to move by diffusion and this maintains the locally large height profile.

It is also worth noting that, for a fixed quantity of surfactant, the initial distribution can be important. It is vital that the surface tension gradient is sufficiently large to overcome the yield stress, or no flow will occur. Ultimately, for any initial distribution which drives a flow the surfactant spreads and the gradient decreases, leading eventually to stationary solutions.

6.1.2. *Effect of n* (*with* $B = 0$)

In order to isolate the influence of shear thinning on the spreading process we remove the yield stress by setting $B = 0$ and examine the effect of decreasing n on the flow profiles. Inspection of the results of a typical simulation, shown in figure 6, reveals that the effect of lowering n ultimately mimics a yield stress. That is, the driving force $\sim \sigma_\eta^{1/n}$ and once the surface tension gradients decrease sufficiently,

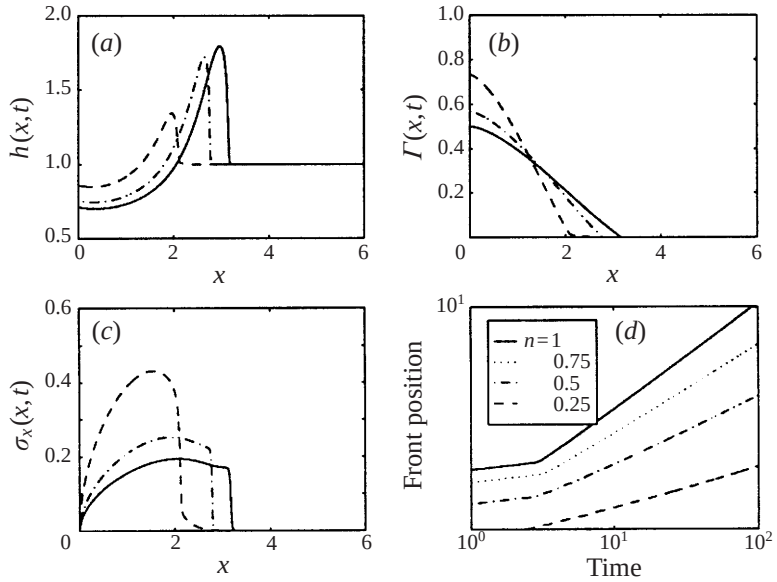

FIGURE 6. The power-law case: simulation for a strip with $Pe = 1000, \beta = 1000, n = 0.5, B = 0$. The solution is shown at times $t = 1$ (dashed), $t = 5$ (dot-dash) and $t = 10$ (solid line). (*a*), (*b*) and (*c*) The evolution of the height of the mucus layer, surfactant concentration and surface tension gradient respectively with time. (*d*) The front position versus time for several values of the power law parameter n.

spreading by Marangoni stresses is significantly retarded, leaving the surfactant no option but to primarily spread by diffusion. The front position scalings shown in figure 6(*d*) follow those deduced in § 5 and illustrate the reduction in the spreading exponent with increasing degree of shear thinning. Another point worthy of comment is the origin of the change in slope at early times in figure 6(*d*): this occurs at the point in time at which the dynamics are no longer governed by the initial conditions, but now take on their long-time self-similar behaviour. The retardation of the front at the surfactant leading edge is further illustrated in figure 6(*a*).

The numerical results depicted in figures 4–6 are for a Cartesian strip geometry and differ only quantitatively from those generated for a drop. Consequently, the basic conclusions are no different in the latter case.

6.2. *Bilayer*

We now explore the more realistic scenario for a pulmonary airway wherein the mucus moves atop the PCL layer; in all the simulations presented in this section the initial height of the PCL is $d_0 = 0.25$. It is expected that the results discussed in this section will bear strong resemblance to those discussed in the single-layer case, with the exception that the unyielded regions can now move atop the PCL. To recap: the velocity field is

$$u(\eta, z, t) = \begin{cases} [\sigma_\eta - B]_+^{1/n}(z - d) + (\mu\sigma_\eta)^{1/n_d} d & \text{for} \quad d < z < h \\ (\mu\sigma_\eta)^{1/n_d} z & \text{for} \quad 0 < z < d, \end{cases} \tag{6.2}$$

such that if the yield stress is significant (or equivalently $n \ll 1$) and $\sigma_\eta \ll B$ then $u(\eta, z, t) \sim (\mu\sigma_\eta)^{1/n_d} d$ throughout the mucus region, that is the velocity is independent

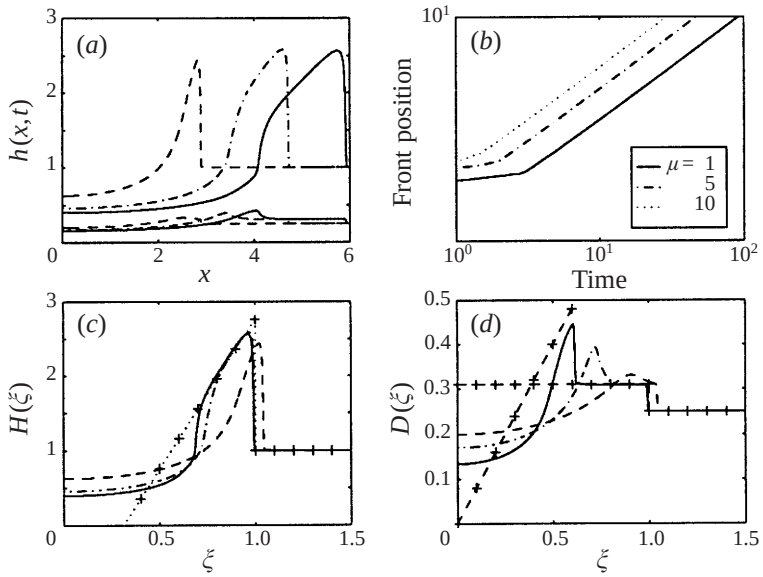

FIGURE 7. The bilayer case: effect of μ. Simulation for a strip with $Pe = 1000$, $\beta = 1000$, $n = n_d = 1$, $B = 0$, $d_0 = 0.25$ and $\mu = 5$. The solution is shown at times $t = 1$ (dashed), $t = 5$ (dot-dashed) and $t = 10$ (solid line) except in (d), where the solid line is for $t = 40$. (a) The height of the mucus layer and (b) the front position for varying values of μ. Similarity scalings are used to show the height in (c) and PCL height together with the similarity solutions (5.8) and (5.9) in (d); all similarity solutions are shown as $\cdots + \cdots$.

of z within that layer. We can then utilize the self-similar analysis, discussed in § 5, to deduce the free-surface profiles.

6.2.1. *Effect of* μ (*with* $B = 0$ *and* $n = n_d$)

Initially we neglect yield stress and examine the case of two Newtonian layers (figure 7*a–d*) allowing the relative viscosities to vary by altering μ. Increasing μ is equivalent to fixing the viscosity of the upper layer whilst decreasing the viscosity of the PCL layer; thus the upper layer ultimately moves over a lubricated base. This explains the results shown in figure 7(b) which indicate that although the fronts still progress with the Newtonian scaling, the coefficients change and the front positions are ahead of the single-layer, $\mu = 1$, case. The other prominent features of the solution are the higher, more sharply peaked, height profiles (the maximum height $\sim 2(\mu^{1/n} d_0)^{1/2} + 1$ for large μ), the more pronounced drop at the origin relative to the the single-layer case and the sharp jump in the PCL height layer. Figure 7(c, d) shows the similarity solution as the dotted line with crosses. In the case of $D(\xi)$ two similarity solutions, (5.8) and (5.9), are shown in figure 7(d): for sufficiently large times (the solid line is for $t = 40$) the secondary peak becomes increasingly aligned with the similarity solution predicted by (5.9). The separation between the PCL height and mucus height also narrows significantly just behind the peak in the height profile, as illustrated in figure 7(c, d). This feature suggests that with the addition of elastic effects the mucus layer may be prone to 'pinching-off' at this point; this would terminate the delivery of surfactant. The sharp peak also naturally leads to queries regarding the stability of these solutions. The effect of allowing the upper layer to shear thin is to yet further exaggerate these features as shown in figure 8(a, b).

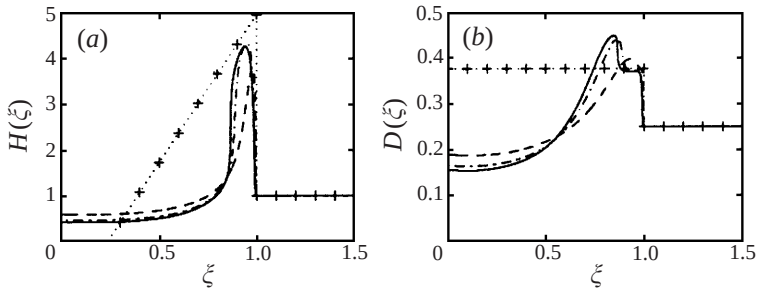

FIGURE 8. The bilayer case: effect of varying n and n_d. Simulation for a strip with $Pe = 1000$, $n = n_d = 0.5$, $\beta = 1000$, $B = 0$, $d_0 = 0.25$ and $\mu = 5$. The solution is shown at times $t = 1$ (dashed), $t = 5$ (dot-dashed) and $t = 40$ (solid line). The similarity scalings are used to display the height of (a) the mucus layer and (b) the PCL height, together with the similarity solutions as the $\cdots+\cdots$ lines.

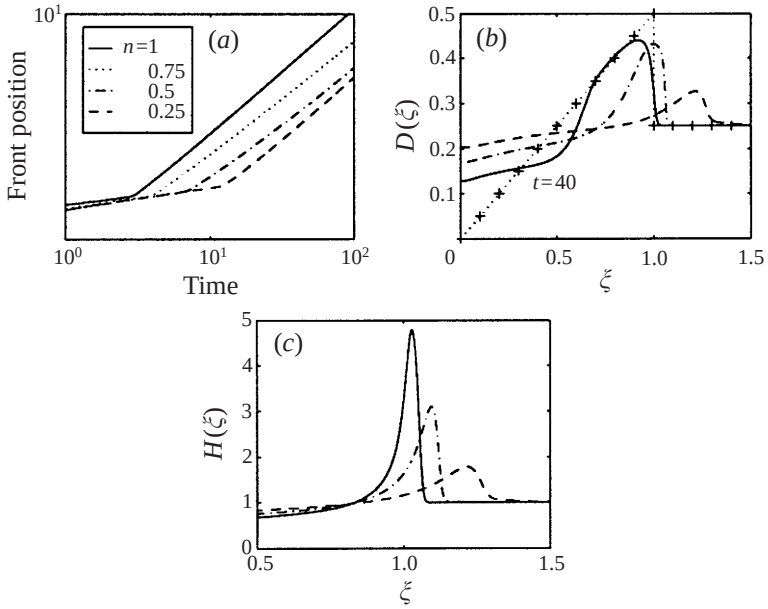

FIGURE 9. The bilayer case: effect of varying n (keeping n_d constant). Simulation for a strip with $Pe = 1000$, $\beta = 1000$, $n_d = 1$, $B = 0$, $d_0 = 0.25$ and $\mu = 1$. The solution is shown at times $t = 1$ (dashed), $t = 5$ (dot-dashed) and $t = 40$ (solid line). (a) The front position scalings as a function of time. (b) and (c) The PCL height and height ($n = 0.25$) profiles versus similarity coordinate; the similarity solution in (b) is shown as $\cdots+\cdots$.

6.2.2. *Effect of $B > 0$ and $n \neq n_d$ (with $\mu = 1$)*

In figure 9 we consider the effect of shear thinning on the spreading process by decreasing n in the upper layer; that is, the PCL layer is Newtonian, but the mucus layer is not. Since the effects of decreasing n and increasing B are to reinforce each other we consider each effect separately. As can be seen from figure 9(a) for sufficiently small n the front position scaling (the slope of the front position curve) rapidly approaches the Newtonian scaling; for larger n this occurs over a longer time scale. The PCL height ultimately follows the Newtonian similarity solution, suitably rescaled to allow for $\mu^{1/n}$, as is evidenced by figure 9(b) (the solutions take longer to tend to the similarity results and here the solid line is for $t = 40$). As in figure

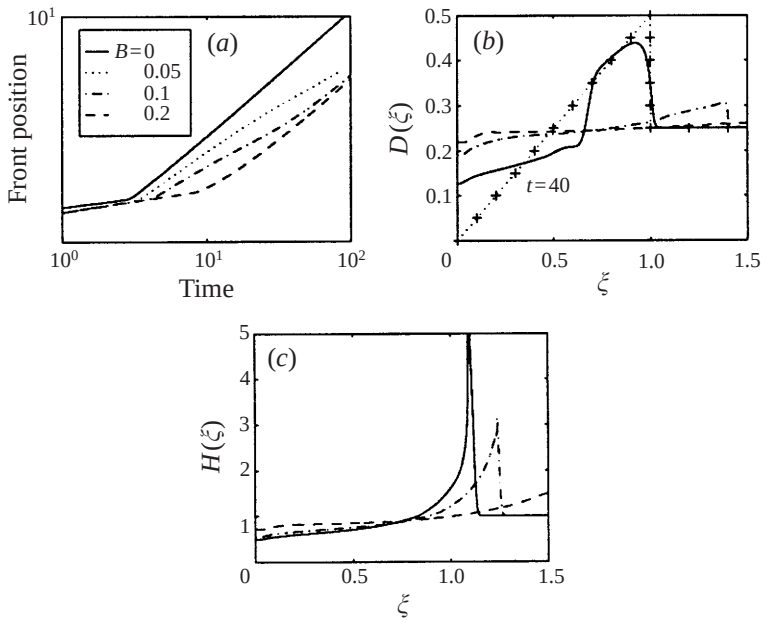

FIGURE 10. The bilayer case: effect of B. Simulation for a strip with $Pe = 1000$, $n = n_d = 1$, $B = 0.2$, $d_0 = 0.25$ and $\mu = 1$. The solution is shown at times $t = 1$ (dashed), $t = 5$ (dot-dashed) and $t = 100$ (solid line). (*a*) The front position scalings as a function of time for varying B. (*b*) and (*c*) The PCL height (evolved to $t = 100$) and height profiles, respectively, versus similarity coordinates with the similarity solution shown as $\cdots + \cdots$ in (*b*).

8(*a*), where we had a single shear-thinning layer, we find that in the bilayer case, with the mucus shear thinning, the height profile becomes large and concentrated into a narrow region. However, it now forms a considerably larger peak which grows over a long time scale, but is ultimately bounded. As in the single-layer case the addition of yield stress leads to very similar results to that of decreasing n as can be clearly seen in figure 10; the choice of B in these figures is marginally less than the value given in table 1: this is to maintain numerical accuracy, as further increasing B leads to even more severe peak formation. This concentrated height peak is rationalized using the discussion from § 5 where it is shown that for $B \gg 1$ or $n \ll 1$ in the similarity coordinates the height equation decouples and is driven by the Newtonian height and surfactant solutions. In the limit as the Péclet number tends to infinity the mucus is completely concentrated at the shock position leading to the formation of a sharp peak at that location. Finally, as far as the rheological effects are concerned, the spreading of a drop of surfactant is qualitatively similar; in the interests of brevity we omit the equivalent figures.

In many ways these numerical solutions are reminiscent of the discussion of mucus clearance by a simulated cough in Basser *et al.* (1989). Although their experiment is not identical to the situation modelled here, it was nevertheless noted that for a current of air flowing over a layer of yield-stress material, a large avalanche of mucus would develop once the mucus simulant layer was stressed enough to either slip on the base or yield; a slipping basal layer of oil strongly accentuated the development of that feature. Although the source of stress for the layer is different here, being due to surface tension gradients, the resultant strongly peaked mucus profiles are qualitatively similar.

7. Concluding remarks

A thorough understanding of surfactant delivery within the lung depends upon a variety of hydrodynamic, physico-chemical and rheological factors. In this, primarily numerical, study we have concentrated upon the influence of two non-Newtonian features of mucus on the spreading of insoluble surfactant on the surface of a mucus–periciliary liquid bilayer: yield stress and shear thinning. These effects had hitherto been unexplored in the literature. The conclusion is that either effect, or a combination of both, have the potential to radically change the spreading rates over those deduced for Newtonian fluids.

The more influential effect in our current study is that of yield stress: for a single-layer system the height profiles and therefore the majority of the deposited surfactant can be frozen in position. That is, the surface tension gradient is not sufficient to drive the flow and the yield strength is sufficient to hold the profiles in place. Thus the surfactant is ultimately transported not by Marangoni stresses, but solely by surface diffusion, that is, very slowly. Substantially decreasing the power-law exponent also has a similar effect; the height profiles are not frozen in position, but their progress is retarded compared to the Newtonian case. The results are less clear-cut for a bilayer as the PCL lubricates the base of the mucus layer and ultimately, even for a thin PCL layer, one obtains the Newtonian spreading rates. The time taken for the solutions to ultimately evolve to this state, however, increases with decreasing flow index, n, and increasing dimensionless yield stress, B, as shown in figures 9(a) and 10(a), respectively. Depending upon the viscosity of the mucus layer, for $n = 1$ and the values in table 1 for $\mathscr{L}, \mathscr{H}$ and $\mathscr{S}$, these times correspond to a dimensional value of λ seconds. For the cases shown figure 10(a) this does not constitute a substantial fraction of the transient transport times of 4–170 s (Espinosa & Kamm 1999) unless the mucus viscosity is extremely large. However, these may grow to be quite significant for higher values of B, which are more representative of mucus rheology. Moreover, different parts of a diseased lung are affected in different ways and for locally thinned regions in the PCL layer, or areas of deep mucus, the single-layer situation will be approached in which spreading is more severely retarded by the effects of yield stress and shear thinning.

All of the simulations in the text have been for a deep layer of mucus, and the PCL height has always been $d_0 = 0.25$; since our estimate is from tracheal values it may be that the mucus layer is thinner in small human airways. We briefly explore varying the depth, and utilize dimensional variables, that is

$$t = \frac{\mathscr{L}^2 \lambda}{\mathscr{S}\mathscr{H}} \tilde{t}, \qquad x = \mathscr{L}\tilde{x},$$

with the tilde denoting the dimensionless variables. We shall use the values for $\mathscr{L}, \mathscr{H}, \mathscr{S}$ given in table 1, and take both layers to be Newtonian ($n = 1$). The viscosity (or more precisely rescaled consistency for a non-Newtonian fluid) is that of mucus, and we shall take this to be highly viscous, 1 Poise (a hundred times that of PCL), so $\mu = 100$. The initial condition is that of equation (6.1). We shall consider the position of the surfactant leading edge as a function of time; the analysis in § 5 gives the front position explicitly in terms of the parameter values. Figure 11 shows the front position for a Cartesian geometry and Newtonian bilayers for values of d_0, the PCL height, of $0, 0.25, 0.5, 0.75, 1$, that is, ranging from completely mucus, to completely PCL. The effect of the PCL is to lubricate the base and this leads to results close to those for PCL alone, nonetheless a deep mucus layer of height 0.75 decreases the distance covered by the front position by a third. Although all of these cases spread with the Newtonian scaling the difference in viscosity and depth leads to a large change in

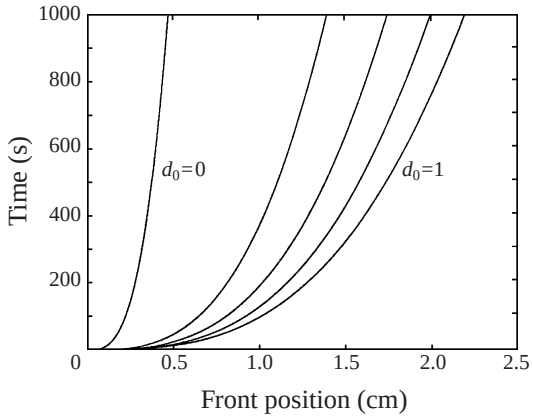

FIGURE 11. The front positions for a Newtonian bilayer in dimensional units for parameters given in the text, and for PCL depths ranging from 0 to 1 in steps of 0.25.

the front position, and changes in the chosen viscosity values can affect comparisons between more realistic and involved lung models (Espinosa & Kamm 1999).

Since experimentally mucus has significantly non-Newtonian characteristics (Basser *et al.* 1989), incorporation of these effects into the recent lung modelling of Halpern *et al.* (1998) and Espinosa & Kamm (1999) may be advantageous. Based on the results of the present work, two major conclusions can be drawn with regard to the practical issues of bolus dispersal: there are several options for liquid delivery and two primary options (Halpern *et al.* 1998) are either as a liquid plug or via slow draining into the lung; if there is substantial mucus present the latter is less likely to generate the large surface tension gradients required to overcome the yield-stress and/or shear-thinning effects, whereas the former should be more effective. It is seen that the latter doses are less effective, and these, or initial ones if substantial endogenous surfactant is present, should strive for rapid insertion to generate surface tension gradients which should overwhelm the resistance of yield stress. Unfortunately, rapid insertion may also have the effect of temporarily blocking the airways, particularly for infants, leading to choking. The mucus rheology associated with specific pulmonary diseases, and the thickness/quality of mucus generated by the lung, are also factors which will influence the efficiency of surfactant delivery. The reason is that an increase in the ratio of the mucus layer height to that of the PCL would again lead to a quasi-single-layer scenario wherein the surfactant spreads over a high-yield-stress material with the adverse consequences already discussed in this study. It may be that different diseases having widely differing mucus quality will require appropriate adjustments in the treatment.

An intriguing aspect of the non-Newtonian case that we have not studied here is the stability, or otherwise, of the pulse-like structures enhanced by yield-stress or shear-thinning rheologies, particularly in a bilayer scenario. These peaks in the mucus film thickness can reach heights well in excess of those reached in the Newtonian case. Although the inclusion of capillary effects may act to smooth these sharp peaks somewhat, their presence may still increase the possibility of liquid bridge formation and hence blocking of the airways. Considering that recent stability analysis of the spreading process has yielded that substantial transient amplification of disturbances can be obtained in the Newtonian case (Matar & Troian 1997, 1999*a*, *b*) the pulses in the mucus layer may also become vulnerable to transverse disturbances giving rise to flow instabilities. The stability of the spreading process, particularly in the limit

of $B \gg 1$ or $n \ll 1$, is therefore worthy of a detailed analysis, and such studies are underway. Finally, although mucus is also known to possess viscoelastic rheological characteristics (King 1980; Basser *et al.* 1989; Yeates 1991), such effects have not been incorporated into the present analysis. These issues are also expected to be significant and will be a subject of future work.

The financial support of an EPSRC Advanced Fellowship and the hospitality of the Isaac Newton Institute, Cambridge is gratefully acknowledged by R. V. C. R. V. C. also thanks Neil Balmforth for many enjoyable conversations on a closely related subject that undoubtedly influenced the current study. Both authors are grateful to a referee for constructive comments regarding the pulmonary application.

REFERENCES

Balmforth, N. J., Burbidge, A. S., Craster, R. V., Salzig, J. & Shen, A. 2000 Visco-plastic models of isothermal lava domes. *J. Fluid Mech.* **403**, 37–65.

Balmforth, N. J. & Craster, R. V. 1999 A consistent thin-layer theory for Bingham fluids. *J. Non-Newtonian Fluid Mech.* **84**, 65–81.

Balmforth, N. J., Craster, R. V. & Malham, S. J. A. 1999 Unsteady fronts in an autocatalytic system. *Proc. R. Soc. Lond.* A **455**, 1401–1433.

Barnes, H. A. 1999 The yield stress – a review or '$\pi\alpha\nu\tau\alpha\rho\epsilon\iota$' – everything flows? *J. Non-Newtonian Fluid Mech.* **81**, 133–178.

Basser, P. J., McMahon, T. A. & Griffith, P. 1989 The mechanism of mucus clearance in cough. *J. Biomech. Engng* **111**, 288–297.

Blom, J. G. & Zegeling, P. A. 1994 Algorithm 731: a moving-grid interface for systems of one-dimensional time-dependent partial differential equations. *ACM Trans. Math. Software* **20**, 194–214.

Borgas, M. S. & Grotberg, J. B. 1988 Monolayer flow on a thin film. *J. Fluid Mech.* **193**, 151–170.

Bull, J. L., Nelson, L. K., Walsh, J. T., Gluckberg, M. R., Schurch, S. & Grotberg, J. B. 1999 Surfactant spreading and surface-compression disturbance on a thin viscous film. *J. Biomech Engng* **121**, 89–98.

Coussot, P. 1994 Steady laminar flow of concentrated mud suspensions in open channels. *J. Hydr. Res.* **32**, 535–550.

Davis, S. S. 1973 Rheological examination of sputum and saliva and the effect of drugs. In *Rheology of Biological Systems* (ed. H. L. Gabelnick & M. Litt), pp. 157–194. Charles C. Thomas, Springfield.

Doelman, A., Kaper, T. J. & Zegeling, P. A. 1997 Pattern formation in the one-dimensional Gray-Scott model. *Nonlinearity* **10**, 523–563.

Dussaud, A. D., Matar, O. K. & Troian, S. M. 1999 Surface profile and spreading speed of an insoluble surfactant film spreading on a thin liquid layer: Comparison between experiment and theory. Submitted to *Phys. Fluids.*

Edwards, D. A., Brenner, H. & Wasan, D. T. 1991 *Interfacial Transport Processes and Rheology*. Butterworth-Heinemann.

Espinosa, F. F. 1991 Spreading of surfactant in a small pulmonary airway. Master's thesis, MIT.

Espinosa, F. F. & Kamm, R. D. 1997 Thin layer flows due to surface tension gradients on a membrane undergoing non-uniform, periodic strain. *Ann. Biomed. Engng* **25**, 913–925.

Espinosa, F. F. & Kamm, R. D. 1999 Bolus dispersal through the lungs in surfactant replacement therapy. *J. Appl. Physiol.* **86**, 391–410.

Espinosa, F. F., Shapiro, A. H., Fredberg, J. J. & Kamm, R. D. 1993 Spreading of exogenous surfactant in an airway. *J. Appl. Physiol.* **75**, 2028–2039.

Gaver III, D. P. & Grotberg, J. B. 1990 The dynamics of a localized surfactant on a thin film. *J. Fluid Mech.* **213**, 127–148.

Gaver III, D. P. & Grotberg, J. B. 1992 Droplet spreading on a thin viscous film. *J. Fluid Mech.* **235**, 399–414.

Grotberg, J. B. 1994 Pulmonary flow and transport phenomena. *Ann. Rev. Fluid Mech.* **26**, 529–571.

Grotberg, J. B., Halpern, D. & Jensen, O. E. 1995 Interaction of exogenous and endogenous surfactant: spreading rate effects. *J. Appl. Physiol.* **78**, 750–756.

Halpern, D. & Grotberg, J. B. 1992 Dynamics and transport of a localized soluble surfactant on a thin film. *J. Fluid Mech.* **237**, 1–11.

Halpern, D., Jensen, O. E. & Grotberg, J. B. 1998 A theoretical study of the surfactant and liquid delivery into the lung. *J. Appl. Physiol.* **85**, 333–352.

Herschel, W. H. & Bulkley, R. 1923 Uber die viskositat und Elastizitat von Solen. *Am. Soc. Testing Mater.* **26**, 621–633.

Huang, X. & Garcia, M. H. 1998 A Herschel–Bulkley model for mud flow down a slope. *J. Fluid Mech.* **374**, 305–333.

Jensen, O. E. 1994 Self-similar, surfactant driven flows. *Phys. Fluids* A **6**, 1084–1094.

Jensen, O. E. & Grotberg, J. B. 1992 Insoluble surfactant spreading on a thin viscous film: shock evolution and film rupture. *J. Fluid Mech.* **240**, 259–288.

Jensen, O. E. & Grotberg, J. B. 1993 The spreading of heat or soluble surfactant along a thin film. *Phys. Fluids* A **5**, 58–68.

Keast, P. & Muir, P. H. 1991 Algorithm 688 EPDCOL – a more efficient PDECOL code. *ACM Trans. Math. Software* **17**, 153–166.

King, M. 1980 Relationship between mucus viscoelasticity and ciliary transport in guaran gel/frog palate model system. *Biorheology* **17**, 249–254.

Liu, K. F. & Mei, C. C. 1989 Slow spreading of Bingham fluid on an inclined plane. *J. Fluid Mech.* **207**, 505–529.

Matar, O. K. & Troian, S. M. 1997 Linear stability analysis of an insoluble surfactant monolayer spreading on a thin liquid film. *Phys. Fluids* **9**, 3645–3657.

Matar, O. K. & Troian, S. M. 1998 Growth of non-modal transient structures during the spreading of surfactant coated films. *Phys. Fluids* **10**, 1234–1237.

Matar, O. K. & Troian, S. M. 1999*a* The development of transient fingering patterns during the spreading of surfactant coated films. *Phys. Fluids* **11**, 3232–3246.

Matar, O. K. & Troian, S. M. 1999*b* Spreading of a surfactant monolayer on a thin liquid film: Onset and evolution of digitated structures. *Chaos* **9**, 141–153.

Matsui, H., Randell, S. H., Peretti, S. W., Davis, C. W. & Boucher, R. C. 1998 Coordinated clearance of periciliary liquid and mucus from airway surfaces. *J. Clin. Invest.* **102**, 1125–1131.

Moriarty, J. A. & Grotberg, J. B. 1999 Flow-induced instabilities of a mucus-serous bilayer. *J. Fluid Mech.* **397**, 1–22.

Quraishi, M. S., Jones, N. S. & Mason, J. 1998 The rheology of nasal mucus: a review. *Clin. Otolaryngol* **23**, 403–413.

Robertson, B. 1984 *Pulmonary Surfactant*. Elsevier.

Rubin, B. K., Ramirez, O. & King, M. 1992 Mucus rheology and transport in neonatal respiratory-distress syndrome and the effect of surfactant therapy. *Chest* **101**, 1080–1085.

Sakata, E. K. & Berg, J. C. 1969 Surface diffusion in monolayers. *Indust. Engng Chem. Fundam.* **8**, 570–575.

Shapiro, D. L. 1989 *Surfactant Replacement Therapy*. A. R. Liss, New York.

Sheludko, A. 1967 Thin liquid films. *Adv. Colloid Interface Sci.* **1**, 391–464.

Sherwood, J. D. & Durban, D. 1998 Squeeze flow of a Herschel–Bulkley fluid. *J. Non-Newtonian Fluid Mech.* **77**, 115.

Silberberg, A. 1983 Biorheological matching, mucociliary interaction and epithelial clearance. *Biorheology* **20**, 215–222.

Sleigh, M. A. 1991 Mucus propulsion. In *The Lung: Scientific Foundations* (ed. R. G. Crystal & J. B. West), Chap. 3.1.4. Raven Ltd, New York.

Stone, H. A. 1990 A simple derivation of the time-dependent convective-diffusion equation for surfactant transport along a deforming interface. *Phys. Fluids* A **2**, 111–112.

Widdicombe, J. H., Bastacky, S. J., Wu, D. X. & Lee., C. Y. 1997 Regulation of depth and composition of airway surface liquid. *Eur. Respir. J.* **10**, 2892–2897.

Wu, R. & Carlson, D. M. 1991 Structure and synthesis of mucins. In *The Lung: Scientific Foundations* (ed. R. G. Crystal & J. B. West), Chap. 3.1.3. Raven Ltd, New York.

Yeates, D. B. 1991 Mucus rheology. In *The Lung: Scientific Foundations* (ed. R. G. Crystal & J. B. West), Chap. 3.1.5. Raven Ltd, New York.